SURVEYOR OBSERVATIONS OF LUNAR HORIZON-GLOW*

J. J. RENNILSON
Division of Geological and Planetary Sciences, California Institute of Technology, Pasadena, Calif., U.S.A.

and

D. R. CRISWELL
The Lunar Science Institute, Houston, Tex., U.S.A.

(Received 13 August, 1973)

Abstract. Each of the Surveyor 7, 6, and 5 spacecraft observed a line of light along its western lunar horizon following local sunset. It has been suggested that this horizon-glow (HG) is sunlight, which is forward-scattered by dust grains ($\sim 10\,\mu$ in diam, ~ 50 grains cm^{-2}) present in a tenuous cloud formed temporarily ($\lesssim 3$ h duration) just above sharp sunlight/shadow boundaries in the terminator zone. Electrically charged grains could be levitated into the cloud by intense electrostatic fields (> 500 V cm^{-1}) extending across the sunlight/shadow boundaries. Detailed analysis of the HG absolute luminance, temporal decay, and morphology confirm the cloud model. The levitation mechanism must eject 10^7 more particles per unit time into the cloud than could micro meteorites. Electrostatic transport is probably the dominant local transport mechanism of lunar surface fines.

1. Surveyor Observations of Lunar Horizon-Glow

Lunar sunset should be a most prosaic event. The Sun is progressively obscured by the western horizon; the terrain darkens as the terminator zone sweeps westward at approximately 15 km h^{-1}; and the solar corona becomes the dominant visible feature following complete obscuration of the eastern solar limb. Lacking an atmospheric suspension of dust or even a sensible lunar atmosphere, lunar sunsets should be completely deficient of the colorful visual effects which accompany terrestrial sunsets. This traditionally accepted preconception of the lunar environment lends considerable mystery to the clear detection of a line of light along the western horizon immediately following sunset by the Surveyor 7, 6, and 5 spacecraft and possibly by Surveyor 1 (Rennilson, 1968; Gault *et al.*, 1968, 1970; Norton *et al.*, 1967). The notation S-7, 6, 5, 1 is used to denote the various Surveyors. Figure 1a, a composite of five S-7 photographs (three daytime and two post-sunset), reveals the general appearance of the horizon-glow (HG) observed at the highland landing site on the northwestern rim of Tycho. The intimate relation of HG to the silhouette of the local western horizon is obvious. Important common characteristics of the S-7, 6, and 5 HG's are: (1) a horizontal extent of approximately 3° on each side of the sunset line; (2) each is

* This work was supported in part by the California Institute of Technology under Grant NGR 05-002-158, and in part by the Lunar Science Institute, which is operated by the Universities Space Research Association under Contract No. NSR-09-051-001 with the National Aeronautics and Space Administration. This paper is Lunar Science Institute Contribution No. 163.

The Moon **10** (1974) 121–142.

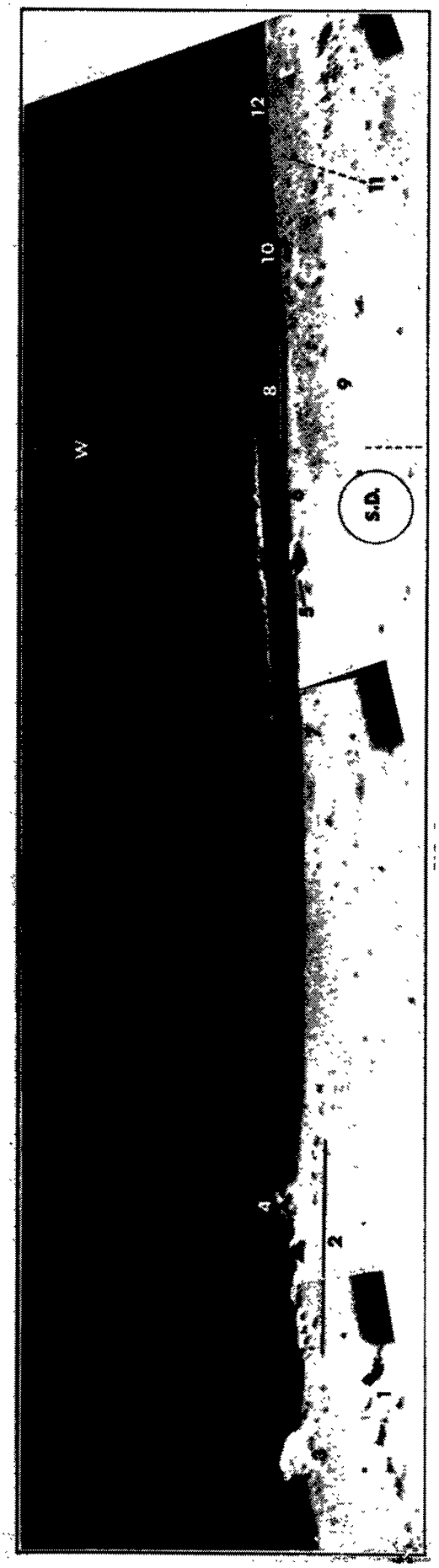

Fig. 1a.

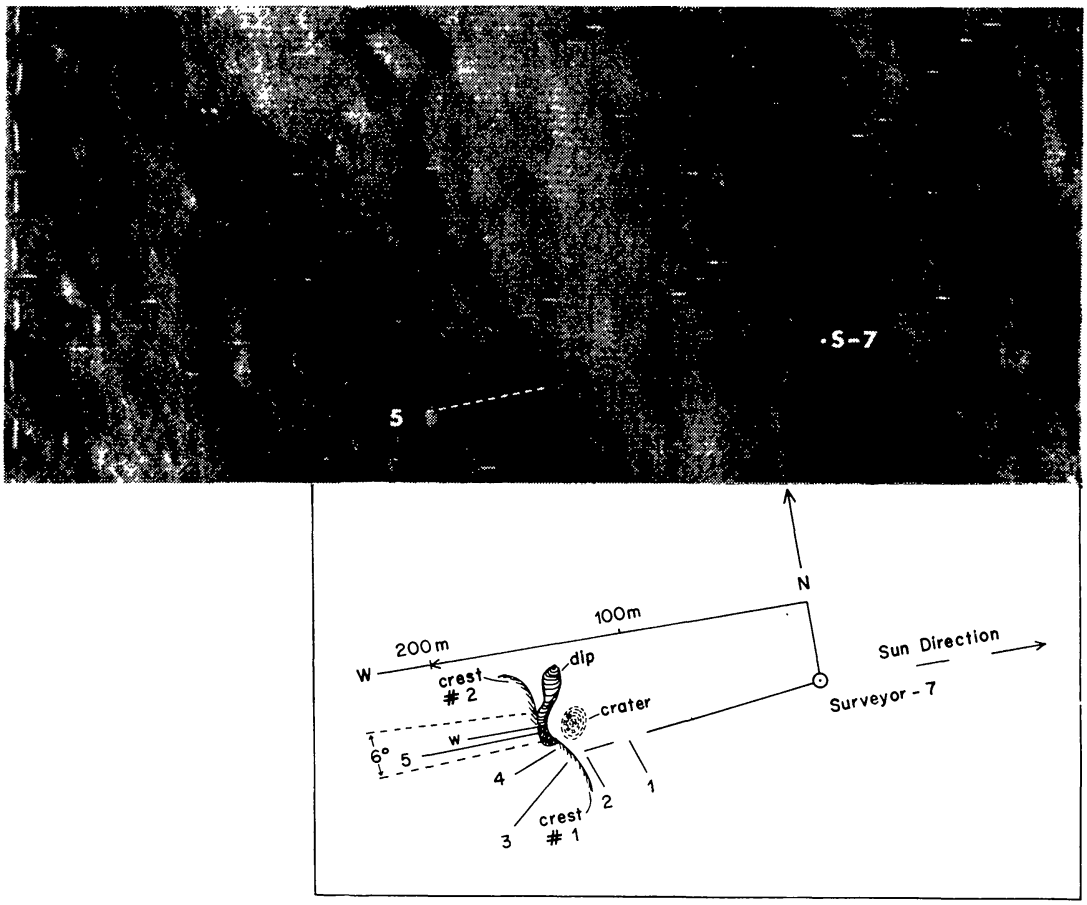

Fig. 1b.

Figs. 1a–b. (a) is a composite of five S-7 photographs. Two nighttime frames of HG (7^h32^m GMT, 23 January) approximately one hour after sunset, and three afternoon photos extending 13.5° along the western horizon. Prominent rocks are numbered and the position of the Sun's disk at the given time is indicated by S.D. Numbers 7 and 12 correspond to creast 1 and 2 in Figure 1b and #11 is the northward extension of crest 1. (b) with insert is part of a Lunar Orbiter III high-resolution frame showing the S-7 site and part of the objects identified in Figure 1a. The insert is at the same scale as the Orbiter photo and directly below the objects marked. Bright areas are slopes facing S-7. The HG gap (i.e., #8 in 1a) is believed to be caused by crest 2 shadowing crest 1. Rock 5 must be at the righthand end of the dashed line but is not resovable in Figure 1b.

closely associated with the western horizon; and (3) each one monotonically decreases in brightness following sunset and all HG's drop below detectability of the respective systems $\frac{1}{2}$ to $2\frac{1}{2}$ h after local sunset (cf. O'Keefe *et al.*, 1968)

Two apparent differences, one large (HG brightness) and one subtle (vertical extent of the HG image), do exist between the S-7 and the S-6 data which affect the selection of a source mechanism to explain HG.

It will be shown that these two 'brightness' and 'morphological' differences can be understood in terms of an HG source region which is approximately 10–30 cm both in vertical extent and in depth along the television line-of-sight. It has been proposed that these HG properties can be understood in terms of visible sunlight which is forward scattered to the Surveyor spacecraft by electrically charged dust grains of a $\simeq 5$–$6\ \mu$

radius ($1\mu = 10^{-4}$ cm) that are electrostatically levitated about partially illuminated rocks or surface irregularities (Criswell, 1972, 1973). The strength of the local electrostatic field E (V cm^{-1}) which must be present in the levitating region is given by $E(\text{V cm}^{-1}) \gtrsim 270\,[a(\mu)]^{1/2}$ and is approximately 660 V cm^{-1} for 6μ grains.

In this particular model the levitating electric field is generated in a two-step process. Photoelectrons of 500 to 1500 eV are emitted due to the absorption of soft solar X-rays with wavelengths less than 25 Å from the sunlit surfaces of rocks or ridges located in the terminator region. Escape of these energetic electrons will continue until sufficient positive charge is left on the rock or sunlit ridge face to force the energetic photoelectrons to return to the general vicinity of the source. A portion of the returning photoelectrons will accrete on the completely dark adjacent areas. These accretion electrons are effectively fixed in location because of the extremely low electrical conductivity ($\eta < 10^{-17}$ to $10^{-16}\ \Omega^{-1}$ cm^{-1} for $T < 300$ K) of the rocks and soils (Olhoeft *et al.*, 1972). Conduction current through the rock can be neglected. A potential difference of at least 500 and conceivably in excess of 1500 V will be generated across the cm-scale boundary between the sunlit and completely dark areas. The significant physical factors are the electrical conductivity (η) of the rocks, flux levels $[\Phi(\lambda)]$ of solar ultraviolet ($\lambda \gtrsim 2000$ Å) and soft X-rays ($\lambda \gtrsim 8$ Å), photoelectron yield $[Y(\lambda)]$ of the rocks and soils in the ultraviolet and soft X-ray ranges, surface reflectance $[R(\lambda)]$ in the mid-ultraviolet, and local surface geometry. The primary evoked motion of levitated grains is localized churning whereas movement of grains out of the regions of intense electric fields will be diffusion-like with smaller grains ($a < 5\mu$) being most likely to be transported over significant distances. Implications of the process for lunar surface effects are discussed in the final section. Churning rates the order of 0.03 g cm^{-2} yr^{-1} are compatible with the S-7 data presented in this paper.

Light scattering is accomplished by large sphere diffraction which produces a lobed intensity $[I(r, \theta)]$ pattern in the antisolar direction as given by Van de Hulst (1957)

$$
\begin{aligned}
&I(r, \theta) = E\,(a^2/r^2)\,x^2\,|J_1\,(x \sin\theta)/x \sin\theta|^2\,,\\
&J_1 \sim \text{1st order Bessel function}\,,\\
&x \equiv 2\pi a/\lambda\,,\\
&a \sim \text{grain radius}\,,\\
&\lambda \equiv \text{wavelength of scattered light}\,,\\
&\theta \equiv \text{scattering angle as measured from antisolar direction}\,,\\
&E \equiv \text{solar illumination (13.7 1m cm}^{-2}\text{)}\,;
\end{aligned}
\qquad \text{(1a)}
$$

$|J_1(x')/x'|$ has its first null value at $x' = x \sin\theta = 3.832$.

The HG falls to zero luminance for $\theta = \theta_o \simeq 3°$ for $\lambda \simeq 0.4$–0.5μ, which is the peak response region of the Surveyor television system. This means a $\simeq 5$–6μ. The next maximum is $|J_1(\simeq 5.2)/5.2|^2 \simeq 4 \times 10^{-3}$. Thus, contributions from $\theta > 3°$ angles (higher order lobes) will be very small. For the same number density of 2μ and 6μ grains the 2μ grains will scatter $(a_1/a_2)^4 = (2/6)^4 \simeq 10^{-2}$ less light.

The observed HG luminance is the result of scattering by all illuminated particles along a given line-of-sight column (total $= ND$, $N \sim$ grains cm^{-3}, $D \sim$ depth scattering region) and is

$$L(\text{candelas cm}^{-2}) = NDI(r, \theta) F(D'), \tag{1b}$$

where $F(D')$ is the fraction of the solar disk illuminating the HG region (refer to Equation (5)).

Secondary ejecta of micrometeorites would not be consistently restricted to the S-7 HG volume, would not produce a steady spray along the horizon line when averaged over more than twenty 0.15 s observing intervals in which the S-7 HG was detected, and would produce only 10^{-7} the required mass churning rate (Hartung *et al.*, 1972; Dohnanyi, 1971; Braslau, 1970). Rozenberg (1970) has presented clear arguments that scattering by a lunar atmosphere cannot be the source mechanism. Regardless of the required immense molecular number density $\simeq 10^{11}$ cm^{-3}, which is 10^6 times more than present on the dark lunar surface, the scale height of the molecules would have to be the order of a few centimeters, whereas reasonable scale heights are the order of 10's of kilometers (Johnson *et al.*, 1972). Finally, diffraction of sunlight by surface grains on the topmost edge of the horizon is not tenable (Gault *et al.*, 1970), due not only to the vertical extent required (10's of cm versus 5×10^{-3} cm for typical surface grain), but also due to the low probability that the 50μ grains on the top edges of the horizons viewed by S-7, 6, and 5 would have remained sunlit $\frac{1}{2}$ to $2\frac{1}{2}$ hours (Figures 4 and 5) after sunset in the general areas (Gold, 1973). It has also been suggested that HG is light which is scattered from the sunward side of slopes forming the eastern horizon of the spacecraft then to the dark sides of the immediately westward slopes and finally to the television system. This is not tenable since HG appears only above and not on the camera size of rocks such as 5 and 10 in Figure 1a. (Refer to Figure 1b insert.) Additionally crest 1 in Figure 1a completely obscures any further western terrain but HG disappears from crest 1 several hours before the eastern slopes of the S-7 site are completely dark (Allen, 1968).

Previous reports on HG have misinterpreted its actual spatial distribution and brightness due to the lack of access to digitally processed data which has been completely corrected for photometric response of the Surveyor systems and for lack of a detailed understanding of how the Surveyor television systems introduced spatial distortion of the HG images when the cameras were operating in the integration mode.

Correct interpretation of the HG source as a vertically extended cloud of dust grains is of crucial importance to understanding many facets of lunar surface science. Albedo variations, trapping of solar wind gases by grains, track damage and track dating of grains, eradication of small craters in the soil, burial and exposure of rocks, homogenization of near surface layers ($\simeq 1$ cm layer thickness), and many other processes depend on how lunar surface material is moved about. The instantaneous columnar mass flow rate required to produce HG is 6×10^7 times greater than can be produced by meteoritic bombardment which is generally accepted heretofore as the only mechanism capable of long-term continuous redistributing of surface material.

Averaged over a lunar month, the total material moved per unit time electrostatically would be 2×10^5 times more in the HG region than by secondary micrometeorites. Thus, the electrostatic process which levitates surface grains to evoke HG must totally dominate the redistribution of very small soil grains in the HG source region and must be seriously considered as the dominant homogenizing mechanism when averaged over larger areas of the lunar surface.

Of the five Surveyor spacecraft, only Surveyor 3 was operationally unable to observe the western sunset horizon. Of the other four Surveyors, three definitely observed HG and S-1 may have detected an isolated patch of HG. This means HG is a moonwide phenomenon which is occurring continuously in the terminator zone and affects in some way every portion of the lunar surface every twenty-nine days for a period of at least two hours (0.003 of a lunar day) and possibly much longer

2. Characteristics of the Surveyor Television System

The Surveyor television system consisted of a vidicon, shutter and iris package, an adjustable focal length lens, a filter wheel containing one clear filter and three color filters balanced for color photography on S-5, S-3, S-1 and polarizing filters on S-6 and S-7, and the viewing mirror. Three modes of operation were utilized – normal, open, and integration. In normal mode, the shutter was open for a total exposure $T \simeq 0.150$ s. The image projected onto the photocathode (11 mm by 11 mm) of the vidicon evoked a pattern of variable resistivity in which low resistivity corresponded to a high light level. Following shutter closure, an electron beam ($\simeq 25\mu$ beam width at the photocathode) scanned the photocathode in 600 lines (18μ line^{-1}). Local photocathode resistivity controlled the instantaneous photocathode electrical potential.

Photocathode potential controlled the frequency modulated telemetry system. The received signals were further processed by digitizing the FM pattern of each line sweep into 684 elements (16μ per element). Each picture element (pixel), which had a diagonal length of 24μ, could then be further computer-processed to correct for geometrical distortion, linearity of signal output versus luminance, and other effects. Following picture readout (which required approximately 1.2 s) a higher positive voltage was placed on the photocathode and the electron beam was swept over the photocathode three times thus neutralizing the previously established photoresistive pattern present on the photocathode. Photo cycle time was 3.6 s. The normal mode was utilized for luminance levels the order of 0.01–3.4 cd cm^{-2} (30–10000 fL). Very sharp images were produced in this mode as there was very little overlap or spreading of the photoresistive patterns over distances of 25μ. Notice in Figure 1a that surface brightness differences (rocks, shadows, etc.) are sharp down to the resolution limit of the photograph even for a rock such as #3 which is framed against the blackness of space.

Open mode was utilized for dimmer scene luminance of $(0.856 \text{ to } 17) \times 10^{-3}$ cd cm^{-2} or 2.5 to 50 fL. The shutter was commanded open and the photocathode was continuously scanned by the electron beam. Thus, each pixel element had an exposure

time of 1.2 s (approximately 8 times more than in normal mode) between readout/erasure passages of the electron beam. Full preflight calibrations of the Surveyor systems were conducted for the normal and open modes of operation.

Integration mode operation was achieved by removing all electrical bias from the photocathode. The shutter was then commanded open and left open until a shutter close command was sent. A potential was then applied to the photocathode and the readout beam was swept over the photocathode. Image erasure was a problem in this mode even after several erasure cycles. Exposure times ranging from 5 s to 200 min were employed. Preflight luminance calibrations were not conducted for this mode. The mode was used only for night operations and was sensitive to extended sources with luminances in excess of 0.28×10^{-5} cd cm^{-2} (0.008 fL). Definite distortions of images, originating in spreading of photoresistive patterns on the photocathode, were apparent in photos of stars and the lunar surface under earthshine.

Photometric calibration was achieved by exposing the TV system to a uniformly diffuse light source which filled the camera field of view (FOV). In calibration, the output signal of each pixel was recorded as the luminance of the calibration source was varied across the dynamic range of the TV system. Equation (2) relates the actual luminance of an object (L_o) to the comparable luminance (L_c) of the calibration source which was required to evoke the same pixel output

$$L_o = L_c \frac{F_o}{F_c} \frac{\mathrm{d}\Omega_c}{\mathrm{d}\Omega_o},$$
$$L_c = K \cdot \text{pixel output (cd cm}^{-2}\text{)}. \tag{2}$$

In Equation (2) F is the luminous flux striking the pixel; $\mathrm{d}\Omega$ is the solid angle subtended by the source as seen from the TV system; 'o' denotes the object; 'c' denotes the calibration source; and K is the calibration coefficient. Pixel output is measured in terms of DN (8-bit digital numbers) which range from DN = 0 (no signal) to saturation (DN $\simeq$ 215 but slightly different for each camera).

This system was calibrated in visual photometric units. All HG photos which are useful for quantitative analysis were taken through the telephoto lens operated at the maximum focal length of 100 mm which produced a 6.43° field of view in a plane along the scan axis of the photocathode. Each pixel had a half-angle FOV in the plane of the scan axis of $\phi_s \simeq \frac{1}{2} \times (6.43°/684) = 4.7 \times 10^{-3}$ deg or 1.69″. This corresponds to a solid angle $\mathrm{d}\Omega_c = \pi \sin^2 \phi_s$(pixel) $= 2.1 \times 10^{-8}$ sr. The diagonal half-angle of each pixel is approximately $\phi_d \simeq 7.02 \times 10^{-3}$ deg (1.2×10^{-4} rad).

Photometry of an extended source whose image fills the pixel, is compatible with the calibration procedure. In Equation (2) $F_o = F_c$ and $\mathrm{d}\Omega_c = \mathrm{d}\Omega_o$ would pertain, thus $L_o = L_c$. As will be presently discussed, it appears that the S-7 HG was an extended source. In addition, the S-7 HG was sufficiently bright that the camera could be operated in the response ranges (normal and open) for which it was calibrated, that is $F_o = F_c$. However, for the S-6 and S-5 HG, these conditions do not appear to have applied.

If the image of a given source is smaller than the pixel, then Equation (2) must be corrected. For an unresolvable circular point source, one would have

$$d\Omega_o\,(\text{circular}) = \pi\, d^2/r^2\,, \tag{3}$$

where $d \sim$ source radius and $r \sim$ TV-source separation. If the object is a line source of unresolvable vertical extent (h) then

$$d\Omega_o\,(\text{line}) = \text{area}/r^2 = (r\phi_d)\, h/r^2 = \\ = h\,[\arcsin\,(d\Omega_c/\pi)]^{1/2}/r \simeq \frac{h}{r}\sqrt{\frac{d\Omega_c}{\pi}}\,, \tag{4}$$

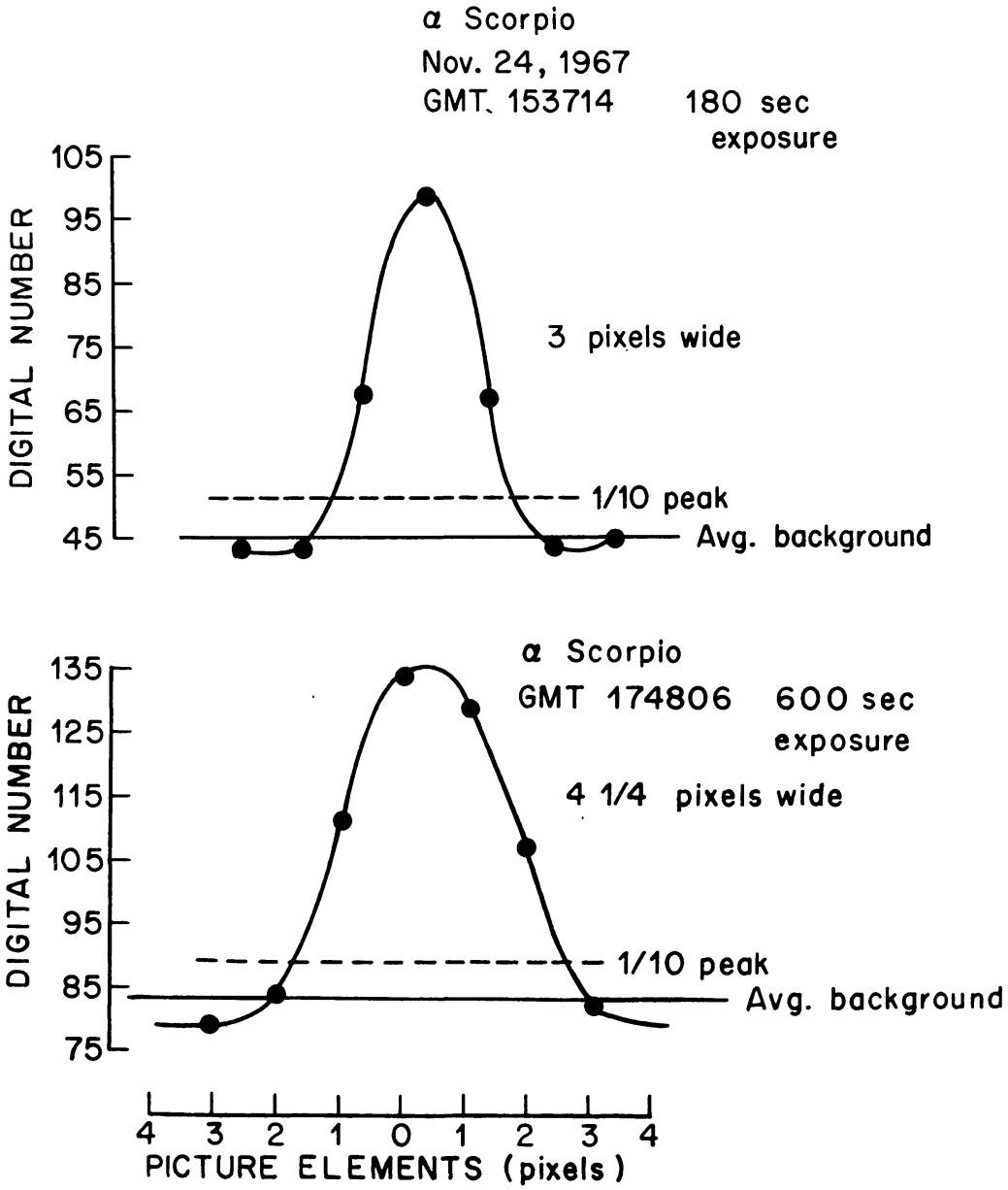

Fig. 2. A plot of digital numbers (DN) of two exposures of the star α-Scorpio (mag. 1.2) as recorded by S-6 after local sunset. The exposure times are shown. Some spreading of the image has occurred.

where $d\Omega_c$ is the solid angle viewed by the given pixel. Due to the geometry of the Surveyor system the western lunar horizon was never parallel to the photocathode scan direction.

Experiments on vidicon systems have confirmed the image spread over several pixels of line sources which are unresolvable in thickness as a function of source luminance (Rennilson, 1969; Thorpe, 1973). For source luminance (L) below the saturation level (L_s) of the television system the image spreads one to two pixels as measured between 1/10 max amplitude contours. For greater luminance, the spread is proportional to the log of the luminance (i.e., 3 pixels at 2 times saturation, 6.5 pixels at 10 times saturation, etc.). The Surveyor 7 HG observations were all obtained for source luminance well below saturation; thus the S-7 HG images with widths in excess of 2 pixels should represent extended sources. For short exposure times (T), it is known that pixel output is actually proportional to LT if $L(T/1\ \mathrm{s}^{-1}) < L_s$. This is called reciprocity. Only limited work was done with the Surveyor television for exposure times comparable to the conditions under which S-6 and S-5 HG measurements were made. A prototype system was checked for image spread (Allen and Salomon, 1970). In the S-6 case, the initial HG observations had $LT > L_s \cdot 1$ s and $T \lesssim 6.8$ s; the bright regions were saturated and definite image spread occurred. After thirty minutes additional observations were repeated for which $LT \gtrsim L_s \cdot (1\ \mathrm{s})$ but $10\ \mathrm{s} < T < 1000$ s. The critical question is whether or not image spread occurred.

Figure 2 illustrates that some spreading did occur. These curves are the distribution of pixel values evoked by the star α-Scorpio as observed by S-6 after local sunset. Image spread increases with increasing exposure time (180 s and 600 s). The α-Scorpio DN values are much less than those of the S-6 and S-5 HG. It is intuitively appealing to think that spreading for a given exposure time is more extensive as L increases. This point will be amplified in the analysis of the S-6 observations.

3. Surveyor 7 Observations

The HG in Figure 1a extends 5.5 deg along the horizon and was approximately centered about the horizon point directly above the solar disk. Notice that the HG lower edge very faithfully silhouetted the rocks and surface irregularities of the horizon to the resolution limits of both the day and night-time photographs. Slight scaling differences occurred during composite production. The HG had a maximum height in digitized maps of the photo the order of 8 pixels or a vertical angular extent 0.11° or 1.9×10^{-3} rad.

Figure 1b is a high-resolution Orbiter-5 photograph of the S-7 site which has been electronically enhanced from telemetry tapes (provided by personnel in the Earth Resources Division, Johnson Space Center) and photographically enlarged. The exact landing site and scaling were based on JPL Technical Report 32-1264 (p. 14).

The prominent rocks 1, 2, 3, and 4 and the crater (9) are identifiable in both figures. Angular separations in Figure 1a are then translated to 1b for locating the source regions (crests 1 and 2) and the position of rock 5. Bright areas in 1b correspond to

slopes facing S-7; conversely, dark areas are locally horizontal or directed away from S-7.

Crest 1 is approximately 150 m from S-7 and crest 2 is 5 to 8 m further westward (refer to insert 1b). Viewing the right-hand side of Figure 1a edge on (parallel to the horizon line) dramatically enhances the terrain contours between crests 1 and 2 (#7 and #12 in Figure 1a). Agreement between the dark areas in 1b and the low areas of 1a is readily apparent. Point 11 of Figure 1a is the continuation of crest 1 between the dip and crater (insert 1b). It is natural to assume the HG gap or shadow zone (#8 in Figure 1a) results from the shadowing of crest 1 by the southern portion of crest 2. However, independent confirmation of the relative heights by stereo-photography or photography at low western sun angles is not available. Clearly, however, the crests are relatively narrow (<1 m). Rock 10 (Figure 1a) is a few meters eastward of crest 2 as is obvious from the presence of its southward directed shadow. HG is present over the top of the rock. This case was specifically considered theoretically by Criswell (1972). Rock 10 is especially significant because the glow above it must be originating in a volume no greater in extent along the TV line-of-sight than the dimensions of the rock top ($\simeq 3$ pixels $\cdot 2.4 \times 10^{-4}$ rad pixel$^{-1} \cdot 1.5 \times 10^{4}$ cm $\simeq 11$ cm). These two observations are important because the HG must be originating from a source volume which is small and definitely not extending many meters or kilometers in the westward direction.

Figure 3a is a digitized portion of the S-7 HG ($6^h\ 15^m\ 44^s$ GMT) above rock 6. The maximum vertical extent is the order of 8–10 pixels. Thus, the height is the order of 30 cm. Figure 3a is based on data obtained in normal mode operation. Saturation occurs for DN > 150. Clearly saturation and, therefore, image spread, is not a problem. Even assuming a 2-pixel spread of the data, the HG vertical extent in this example would be at least 20 cm or greater.

Maximum luminance in 3a is the order of $L_o \simeq 0.26$ cd cm^{-2} (760 fL). Using Equation (1a–b) with $E = 13.7$ lm cm^{-2}, $a \simeq 6 \times 10^{-4}$ cm, $\lambda = 0.5 \times 10^{-4}$ cm, $\theta = 0.5°$, $D \simeq 10$ cm, $F(D) \simeq 0.65$ we obtain a columnar number density $N \cdot D \simeq 50$ grains cm^{-2}.

Criswell (1972) provided a digitized representation of the S-7 HG about rock 5 showing a vertical extent of 4–8 pixels. This figure included an insert of a saturated laser beam image which displayed only a 2-pixel spread, thus demonstrating again that the S-7 HG was an extended source.

If the glow were due to diffraction or scattering by an unresolvable top layer of dust then L_o would be much higher. Using Equation (4) for a line source with $h \simeq 5 \times 10^{-3}$ (comparable to the average diameter of the dust grains), $r \simeq 1.5 \times 10^{4}$ cm, and $d\Omega_c \simeq 2.1 \times 10^{-8}$ sr one has

$$L_o(\text{unresolved}) \simeq L_o(\text{resolved}) \times (r/h)\,(d\Omega_c/\pi)^{1/2}$$
$$\simeq 65 \text{ cd cm}^{-2} \quad \text{or} \quad \simeq 1.9 \times 10^{5} \text{ fL}.$$

An unresolved line of this luminance would evoke a 6–7 pixel image spread across the 1/10 DN saturation contours and a central line of saturated pixels (DN > 180).

C7, ID = 1350, GMT. 23-06-51-44 F-06.6 FILTER 1 C
ATE 90 DEGREES CLOCKWISE IHL

SAMP E	1		3		5		7		9		11		13		15		17		19		21		23		25		27	
1	3	3	3	3	3	3	1	3	1	3	3	3	3	3	3	3	6	3	3	3	3	3	1	1	1	3	6	6
2	6	6	3	3	3	3	3	3	3	1	6	3	1	3	6	6	6	3	3	3	3	3	3	3	3	3	3	3
3	17	9	9	3	6	6	6	6	6	3	3	3	1	3	3	6	1	3	6	6	6	1	3	3	3	3	3	1
4	39	23	15	9	3	6	6	6	3	3	3	6	3	6	6	6	6	3	6	3	3	3	3	3	1	3	6	3
5	59	42	23	15	6	6	6	6	6	3	6	6	15	20	26	23	17	12	6	6	3	3	1	1	6	3	3	3
6	59	56	34	20	12	6	9	9	15	9	9	12	45	56	62	62	50	26	9	9	3	6	3	3	3	6	6	6
7	61	56	44	28	17	26	33	33	39	26	23	34	65	68	68	71	71	42	23	12	9	6	6	3	3	3	3	3
8	58	58	53	42	42	56	62	62	62	53	56	62	65	62	67	68	71	59	31	17	12	6	6	3	3	1	3	6
9	58	58	56	56	58	59	65	65	65	61	64	65	64	67	64	68	72	68	47	31	20	15	12	9	9	12	6	6
J	53	53	50	61	61	61	61	61	61	64	64	64	67	67	67	67	70	70	70	61	50	45	31	26	26	23	15	9
L	15	22	28	53	58	61	61	64	64	67	64	64	50	44	56	67	70	70	73	73	73	70	67	61	61	58	42	34
[illegible]	9	0	4	17	44	56	56	64	61	64	61	50	17	12	30	70	72	70	73	73	70	73	70	73	73	73	76	67
[illegible]	10	0	3	3	5	15	17	36	36	42	28	12	0	0	15	70	70	73	70	73	73	70	73	73	73	76	73	76
[illegible]	4	0	2	2	0	0	0	0	0	0	0	0	0	0	2	36	64	67	73	73	70	73	73	73	73	76	76	76
[illegible]	2	2	2	0	0	0	0	0	0	0	0	0	0	2	0	0	15	28	47	58	61	56	67	70	73	76	76	76
[illegible]	4	4	2	2	2	0	0	0	0	0	0	0	0	0	0	0	0	0	9	15	12	23	31	39	53	73	76	
[illegible]	7	4	4	2	2	2	2	2	0	0	2	2	2	2	0	0	0	0	0	0	0	0	0	0	0	39	70	
[illegible]	4	4	2	2	2	2	2	2	2	2	2	2	2	2	0	0	0	0	0	0	0	0	0	0	0	0	26	
[illegible]	4	4	4	4	4	4	4	4	4	4	4	4	4	4	4	4	4	4	4	4	4	4	4	4	4	4	4	

LUNAR SURFACE

Fig. 3a.

C6, ID = 20007, GMT. 328-14-15-26. C
T CORONA IHL

SAMP E	1		3		5		7		9		11		13		15		17		19		21		23		25		27		29	
1	66	66	66	62	69	69	69	69	73	73	77	77	80	77	80	80	88	88	92	92	92	92	92	92	95	95	95	95	95	104
2	62	66	70	70	70	70	77	73	73	73	77	77	80	80	80	88	88	88	88	92	92	95	95	95	95	99	99	104	104	99
3	66	70	70	70	74	74	70	74	78	82	78	80	80	84	84	88	88	88	95	99	95	99	104	99	99	104	104	104	108	113
4	66	70	74	74	74	74	78	82	82	80	80	84	84	84	88	92	92	95	95	99	99	104	108	108	113	108	108	108	113	113
5	70	66	74	74	78	78	78	78	82	80	84	84	88	84	88	95	95	95	95	104	108	104	108	113	113	108	113	117	113	113
,	70	70	74	78	74	82	78	82	80	84	84	88	88	88	95	95	99	104	104	104	108	113	113	108	117	117	113	117	117	117
7	74	74	74	78	82	82	82	82	84	84	88	92	95	95	99	99	104	104	108	108	108	117	113	117	117	117	122	122	122	122
8	74	74	78	82	86	82	86	90	88	92	92	95	92	99	104	108	104	108	108	113	117	117	117	117	134	122	134	134	146	157
9	82	78	82	86	86	86	86	94	92	95	92	95	95	104	108	108	113	108	117	117	117	122	122	134	146	146	157	157	157	169
0	78	82	86	90	90	86	94	90	95	95	99	99	99	104	108	113	113	113	122	122	134	134	134	146	157	169	169	181	193	205
1	82	82	86	86	86	94	94	95	99	95	99	99	104	113	108	113	117	117	134	134	134	146	146	169	181	181	205	216	216	228
2	82	86	86	86	90	90	98	98	102	104	99	104	108	108	113	113	117	122	146	146	134	157	169	193	193	193	205	252	255	252
3	82	86	90	90	94	98	98	102	102	104	104	104	104	113	117	122	134	122	157	157	181	181	181	205	205	228	240	255	255	255
4	86	86	90	94	94	98	102	102	107	111	108	108	113	117	122	122	146	157	169	181	193	205	216	228	216	240	255	255	255	255
5	94	94	94	98	98	98	107	107	111	111	111	117	117	122	122	146	157	169	181	193	216	228	240	240	252	252	252	255	255	240
6	94	94	98	102	102	111	111	111	111	116	125	117	122	134	146	169	169	181	216	228	240	255	255	255	252	255	255	228	169	157
7	94	98	98	98	111	111	111	111	116	120	120	136	146	157	157	181	205	228	240	252	255	255	255	255	255	255	240	169	92	69
8	94	94	102	102	102	116	116	116	120	120	125	170	157	169	181	205	228	240	252	255	255	255	255	255	255	255	240	228	146	73
9	98	94	98	107	107	116	116	120	125	125	159	170	170	193	205	228	240	252	255	255	255	255	255	255	240	216	169	95	59	40
0	94	98	102	107	116	116	116	125	125	147	170	192	205	216	228	255	255	255	255	255	255	255	255	240	193	157	99	62	46	31
1	98	98	102	102	107	116	120	125	136	170	192	216	228	252	255	255	255	255	255	255	255	255	240	205	181	122	92	66	40	24
`	98	102	107	107	116	125	125	147	159	181	216	240	255	255	255	255	255	255	255	255	240	193	169	113	92	66	43	21	11	0
3	98	102	107	116	125	136	136	146	181	216	228	255	255	255	255	255	255	255	253	253	202	169	122	99	88	62	31	14	5	11
4	102	107	111	125	125	147	169	181	205	228	252	255	255	255	255	255	255	255	222	181	130	112	92	73	46	17	11	7	7	5
5	98	107	116	120	136	159	192	205	228	252	255	255	255	255	255	255	228	191	161	116	95	80	53	28	17	14	5	0	0	0
6	98	102	111	136	159	173	193	228	240	240	255	255	240	216	216	146	116	95	77	59	37	17	11	11	0	5	4	4	4	5
7	90	102	116	122	146	181	193	205	205	228	228	193	169	122	113	95	77	62	34	21	17	14	7	7	7	4	4	4	4	4
8	104	117	117	122	157	134	134	113	122	122	113	95	92	84	69	53	31	21	17	14	11	7	4	7	4	4	4	4	5	4
)	146	157	157	157	134	104	84	53	43	50	56	56	53	40	31	21	17	14	11	7	11	4	7	4	4	4	4	4	4	4
0	205	205	181	157	134	84	40	17	21	21	28	21	21	17	14	11	11	7	11	11	7	4	7	4	4	4	4	4	5	4
1	205	169	134	146	84	40	14	11	11	11	14	14	11	11	7	11	11	7	7	7	4	4	4	4	4	4	4	4	4	4
2	122	113	104	92	46	17	11	14	14	7	11	11	11	7	7	7	7	7	7	7	4	4	4	4	4	4	4	4	4	4
3	73	53	56	43	21	11	11	11	7	11	4	4	7	4	7	4	4	7	7	7	4	4	4	4	4	4	4	4	4	4
4	50	28	24	21	14	4	4	4	4	4	4	4	4	4	4	4	4	4	4	4	4	4	4	4	4	4	4	4	4	4
5	24	14	14	17	11	4	4	4	4	4	4	4	4	4	4	4	4	4	4	4	4	4	4	4	4	4	4	4	4	4
,	11	4	7	7	4	4	4	4	4	4	4	4	4	4	4	4	4	4	4	4	4	4	4	4	4	4	4	4	4	4
[illegible]	4	4	4	4	4	4	4	4	4	4	4	4	4	4	4	4	4	4	4	4	4	4	4	4	4	4	4	4	4	4

LUNAR SURFACE

Fig. 3b.

Figs. 3a–b. (a) Digitized (8-bit) map of S-7 HG over rock 6 at 0.75 h after sunset (best estimate). Multiply DN's by 3.4×10^{-3} for absolute luminance in cd cm^{-2}. Saturation occurs only if DN$>$150. (b) Digitized (8-bit) map of S-6 HG above sunset point at 1.1 h after sunset (best estimate). Multiply DN's by 0.091×10^{-4} for apparent luminance in cd cm^{-2}. Saturation occurs if DN$>$180. See Figure 7 for location of digitized area.

Such a contour is not observed. This point will be raised again when the S-6 observations are discussed.

The L_o curve in Figure 4 is the temporal decay of S-7 HG luminance above rock 5 (Figure 1a) versus time after the first photo of the HG. Each solid data point actually

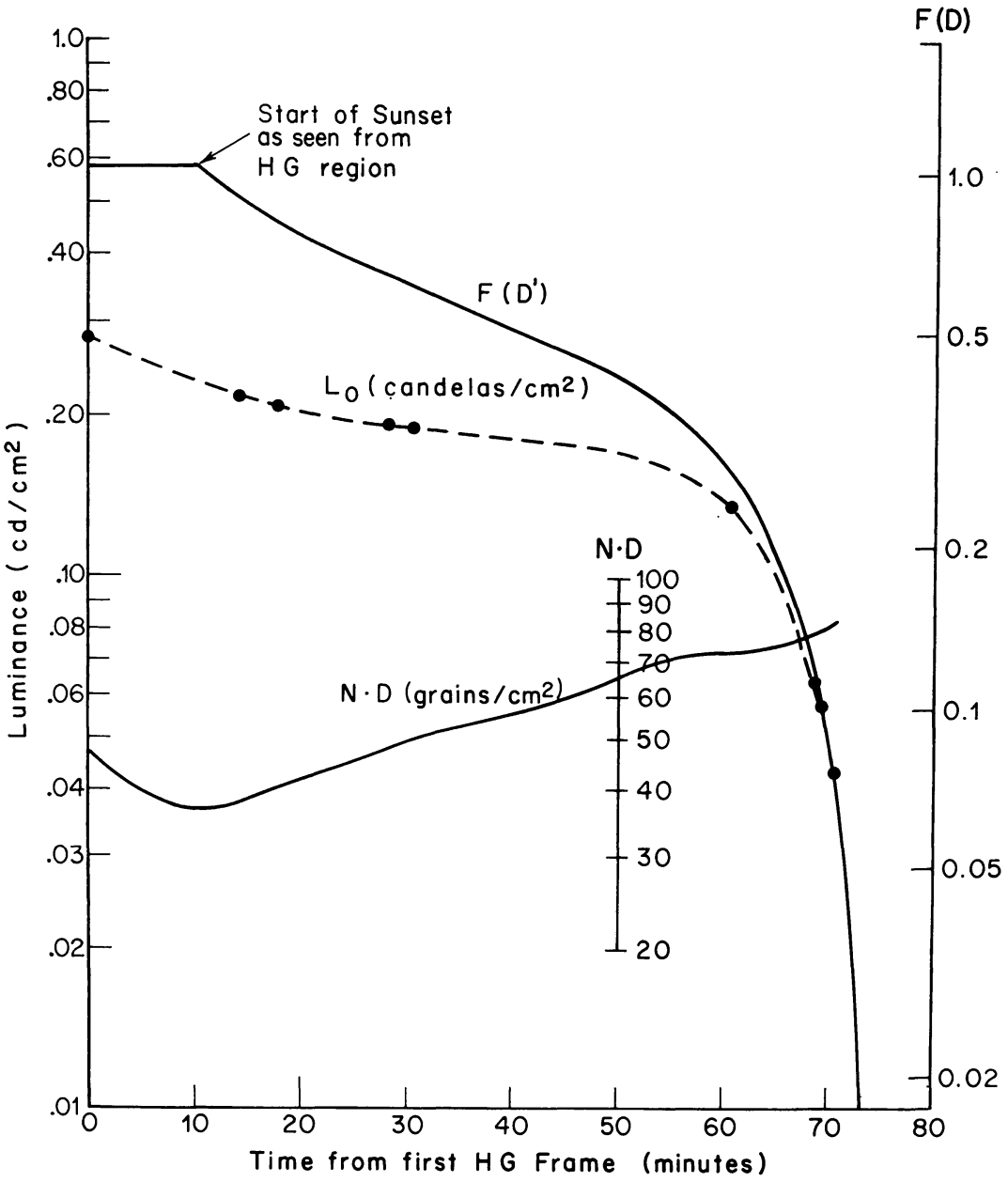

Fig. 4. Plot of the S-7 HG luminance L_o as a function of time from the first HG photograph. Included on the graph are plots of the columnar grain density ($N \cdot D$) as a function of frame time. The curve $F(D')$ is the fraction of solar disk illuminating the HG source region and is adjusted to match the sharply decreasing right side of the L_o curve.

represents four observations taken through polarizing filters. The differences in luminances were statistically unresolvable. Thus polarization, if it existed, was less than 4%. Television sunset for S-7 preceded start of sunset for crests 1 and 2 by approximately 20 min. The temporal variation of the columnar dust density can be obtained by correcting E in Equations (1a, b) for gradual obscuration of the solar disk by a distant westward flat plane. Equation (5) is the correction factor $[F(D')]$ specifying the fractional illumination of the solar disk versus D', where D' is the fraction of

the solar diameter between the top of the solar disk and the obscuring plane ($D'=1$, Sun's lower edge just on the plane and $D'=0$, Sun's upper edge just below plane)

$$F(y) = [F_o(-1)]^{-1} \left\{ \left(\frac{1-u}{\pi} \right) [\cos^{-1} y - y\sqrt{1-y^2}] + \right.$$
$$+ u/6[2 - y - y^3] - (v/6\pi)[3\cos^{-1} y - \sqrt{1-y^2} \cdot$$
$$\left. \cdot (y + 2y^3)] \right\}, \tag{5}$$

where $y=-2D'+1$ and $u=0.95$ and $v=0.2$ are appropriate to limb darkening of the Sun at 0.5μ (Allen, 1955).

The $F(D')$ curve is adjusted on the graph to match the right-hand portion of the L_o curve. The $N \times D$ curve is the columnar grain density in the HG region calculated from Equation (1) using the top curves and assuming $\lambda=0.5\mu$, $a=6\mu$, and $\theta \simeq \frac{1}{2}°$. $N \times D$ ranges from 37 to 84 grains cm^{-2} and monotonically increases ($t>10$ min) as sunset in the HG source region approaches completion. This behavior is in qualitative agreement with the electrostatic levitation model. One expects a monotonic decrease of the light scattered into the dark, negatively charged regions. The scattered mid-ultraviolet evokes a leakage current of low energy photoelectrons which discharges these regions. The u and v values (refer to Equation (5)) for calculations of time decay of the photoelectrons which evoke discharge currents should actually be adjusted for the 1500–2500 Å solar emissions. There is progressively less discharge as sunset approaches and therefore the electric fields become more intense until final obscuration of the Sun cuts off the source of solar X-rays which drive high energy photoelectron ejection (Criswell, 1973). Solar X-rays are actually generated approximately 50000 km above the photosphere. The Sun can exhibit limb brightening in the X-ray region rather than limb darkening as in the mid-ultraviolet. Thus, high energy photoelectron ejection can often continue in the HG source region for 5–10 min after the sources of mid-ultraviolet photons are completely obscured. The initially high value $N \cdot D \simeq 47$ at the first HG observation may either be real or result from a second order effect due to the angular extent of the Sun which would affect the choice of θ in Equation (1a).

The steady increase of $N \cdot D$ by a factor of 2 in Figure 4 implies that dust motion continues in the HG source region after sunset. Detailed modeling of each source region geometry is required to estimate how long dust motion continues after complete sunset. At least an additional hour seems reasonable in terms of the continuous increase of $N \cdot D$ in Figure 4 and is consistent with results in Figure 5. The total mass churned each year (M_c) by this process is $M_c \simeq 0.03$ gr cm^{-2} yr^{-1} to a depth $d_c \simeq 10^{-2}$ cm. These figures are an order of magnitude higher than presented previously and indicate that over monthly or yearly averages at least 10^4 times more material in these regions will be churned electrostatically than by micrometeorites (Criswell, 1972).

The S-7 curve (Figure 5) contains two additional HG points (A and B) correspond-

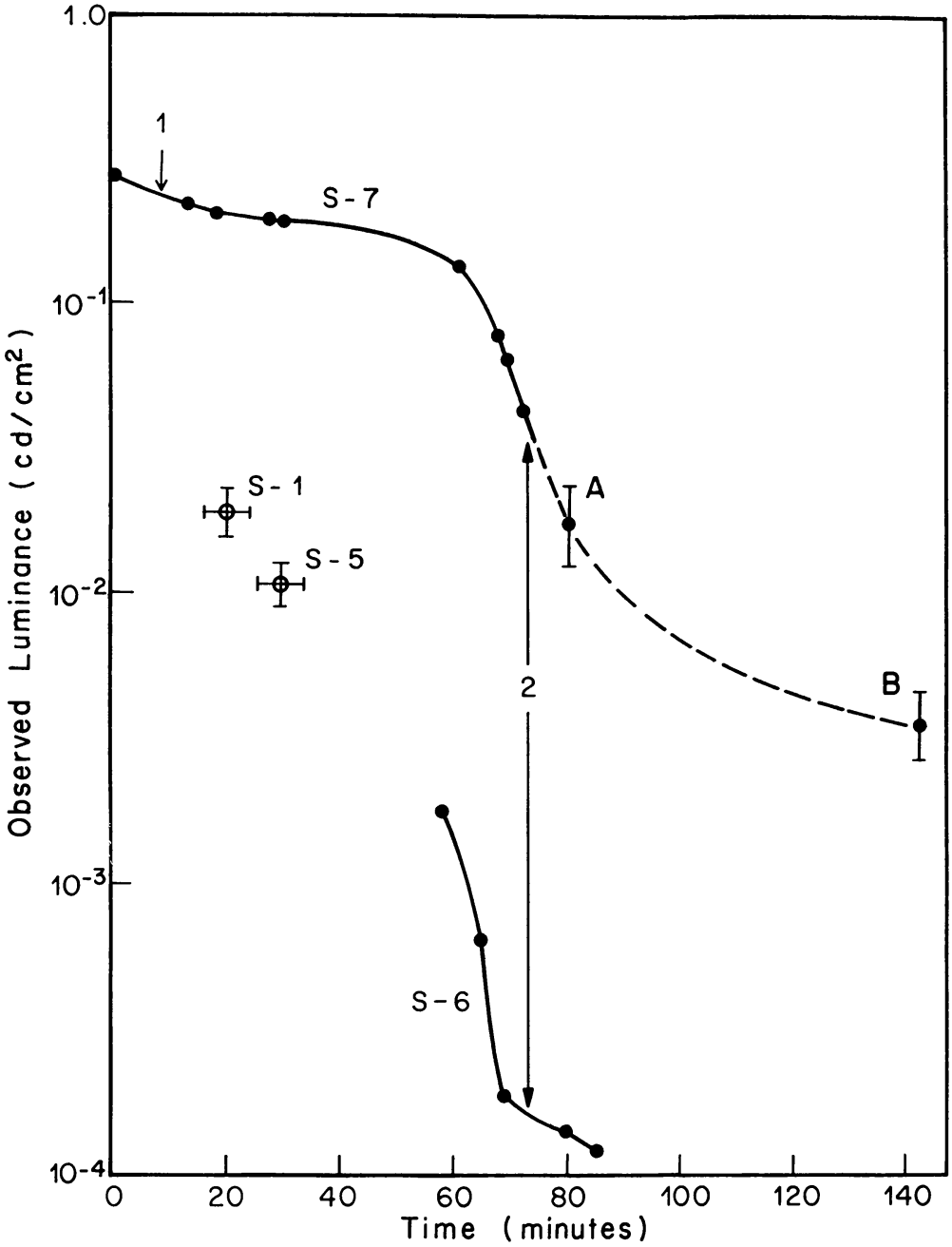

Fig. 5. Is another plot combining the temporal decay curves of S-7 and S-6 HG. The beginning frames for S-1 and S-5 are also included with uncertainty bars relating to luminance and exact time. Two points, marked A and B, are HG still visible in frames at 0741 and 0844 GMT, but with the signal close to the noise level. The period of sharp decay of S-7 (mark ≠ 2) corresponds well with that of S-6.

ing to 80 min and 143 min after the first S-7 HG observation. These observations were obtained at very low signal levels for the particular operating mode of the television (open and f/10.4) and are of limited utility for computation of $N \cdot D$ due to observational uncertainty and lack of knowledge of $F(D)$. However, they definitely occur after complete sunset in the HG region (point 2) and must be due to forward scattering by grains well above the surface (>20 cm). A shadow zone will be present from the

TABLE I

Color plate

Color hues	Digital number group I	Luminances [cd cm^{-2} × 10^{-2}] group II	group III
1	0–11	0– 0.76	0– 0.007
2	12–18	0 76– 0.93	0.007– 0.011
3	19–26	0.93– 1.15	0.011– 0.017
4	27–33	1.15– 1.5	0.017– 0.028
5	34–40	1.5 – 1.81	0.028– 0.045
6	41–48	1.8 – 2.26	0.045– 0.071
7	49–55	2.3 – 2.8	0.071– 0.115
8	56–63	2.8 – 3.5	0.115– 0.186
9	64–70	3.5 – 4.4	0.186– 0.29
10	71–77	4.4 – 5.4	0.29 – 0.46
11	78–84	5.4 – 6.7	0.46 – 0.75
12	85–92	6.7 – 8.3	0.75 – 1.20
13	93–99	8.3 –10.3	1.20 – 1.91
14	100–106	10.3 –12.9	1.91 – 3.0
15	107–114	12.9 –16.2	3.0 – 4.8
16	115–121	16.2 –20.2	4.8 – 7.6
17	122–128	20.2 –25.2	7.6 –12.0
18	129–135	25.2 –33.0	12.0 –19.5
19	136–144	33.0 –39.0	19.5 –30.8
20	145–255	39.0 –49.0	30.8 –49.8

surface to a few tens of centimeters above the surface by the last detection of S-7 HG. This residual glow must originate from grains smaller than 6μ in radius or higher order diffraction lobes of 5–6μ grains since the angular extent of the glow increases in the latter portion of the HG activity (Figure 6-II). Spatial details are not readily apparent in the analog or digital versions. The drop of L_o at point 2, which clearly corresponds to surface sunset in the source region, means that surface grains can no longer be illuminated. Existence of the weak persistent glow, therefore, completely rules out diffraction or scattering by surface grains as the HG source and absolutely requires a vertically extended source. [Note: See frontispiece for Figure 6]

Group II (Figure 6) consisting of five frames of S-7 HG, shows the temporal decay and shift of the maximum luminance within the HG. The scale is logarithmic and its values are listed in Table I. The latter effect is caused by the southward motion of the Sun's position with time. The top edge of the glow changes with time whereas the bottom edge faithfully silhouettes the horizon. The first frame at 0 min, was taken only a few minutes after television sunset, and the last frame corresponds to sunset as viewed from the source region of the horizon-glow. In the bottom frame, the glow expands laterally and becomes more diffuse. This occurs because the camera is detecting only the very faint light scattered into the side lobes of the large sphere diffraction patterns and the wider main scattering lobes of smaller particles.

In summary, Surveyor 7 provided high-quality data ($F_o = F_c$, $d\Omega_o = d\Omega_c$) which

demonstrated that HG must be due to forward scattering of sunlight by a vertically extended source ($h \gtrsim 10$ cm) of suspended dust grains. Intercomparisons with the S-6, 1, and 5 data are presented in the following sections.

4. Surveyor 6 Horizon-Glow

Two factors are important in understanding S-6 HG. First, only the very late portions of the glow were detected, and secondly, the television system did not spatially resolve the glow. Figure 5 presents the S-6 and 7 data on a common time base. Based on estimates of local sunset time, the first S-6 HG was observed approximately 68 min after the start of sunset. Probably only the top of the dust cloud was illuminated (height $\gtrsim 20$ cm). The S-6 HG generally corresponds to source-region sunset of the S-7 HG, about point 2. There is a general matching between the lower boundary of the S-6 HG and the western horizon (Figure 7). Horizon details (i.e., rocks, ridge features) are not present in the S-6 photos as they are in the S-7 photos (Figure 1a). This is true because the S-6 horizon is approximately 2 km from S-6, that is ten times farther than for S-7 (R. Batson, personal communication). The S-6 television system would have had a spatial resolution no better than 840 cm^2 or 30 cm in vertical extent which means the S-6 HG was probably not resolved spatially. The S-7 HG had a height of 10–20 cm on the average. Geometric correction factors (Equations (3), (4)) must be applied to the observed luminance. If a point source is assumed ($d \simeq 10$ cm) $d\Omega_c/d\Omega_o \simeq 2.67$ and for a line source ($h \simeq 10$ cm) $d\Omega_c/d\Omega_o \simeq 5.1$. The brightest position of S-6 (apparent) $\simeq 1.8 \times 10^{-3}$ cd cm^{-2} adjusts to $L_o \simeq 4.8 \times 10^{-3}$ (point) and to 9×10^{-3} (line) cd cm^{-2} which is comparable to the range of late stage S-7 luminance ($L_o \simeq 6 \times 10^{-3}$ cd cm^{-2}) but not to an S-7 luminance corrected to an illuminated line of surface grains ($\simeq 65$ cd cm^{-2}). The S-6 intrinsic brightness is systematically lower than that of S-7 by a factor of 5 to 10.

Details of surface geometry in the S-6 source region will govern the exact temporal decay of the HG. Thus, one would not necessarily expect exactly the same S-6 and S-7 intrinsic brightness at the same times along the decay curve. These considerations could account in part for the factor of 10 difference in S-7 and S-6 intrinsic brightnesses about line 2 in Figure 5.

Group I (Figure 6) shows one example each of a S-7 and S-6 horizon-glow normalized to their brightest internal DN. The color scale is linear and given in Table I. The luminance distribution in each HG is different. The S-7 HG is clearly defined and consists of larger areas of constant color hues (same luminance) than is the case in the S-6 HG. Conversely, the S-6 HG is amorphous and clearly contaminated by the solar corona.

Figure 3b is the digital map (linear luminance scale) of the S-6 HG region indicated in Figure 7. Both representations are deficient of the detailed structure present in S-7. The S-6 HG is reasonably smoothly distributed along the horizon, but is saturated (DN > 180) in the central portion. Several factors indicate that the S-6 HG was unresolved: the camera was operated in the integration mode which tended to result in

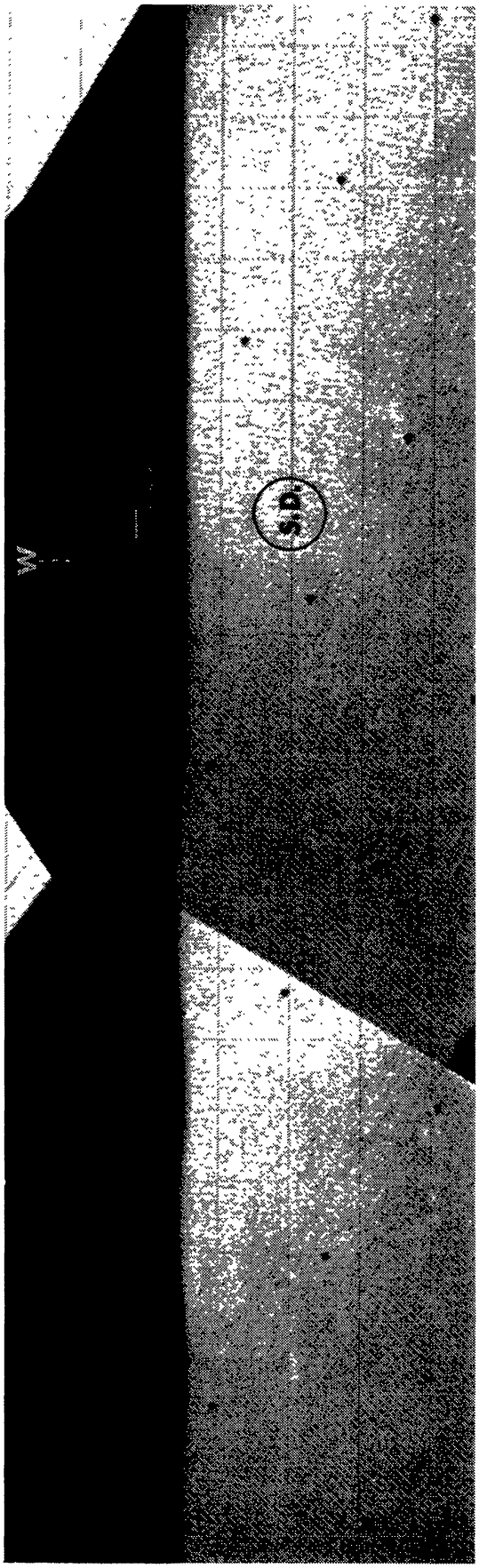

Fig. 7. Is a horizon composite of the S-6 similar to Figure 1a. Vertical separation between the HG and horizon was deliberately introduced in production of this composite. The white line indicates the section of S-6 HG which is presented in digital form in Figure 3-b.

electronic image smear at low light levels (stellar images displayed similar image broadening); at very low light levels the solar corona was as bright as the central portion of the HG and produced a mixture of coronal and HG signals; and as previously noted, the HG map contained no detailed structure. In the central portions of the HG, that is near the sunset line, the solar corona and HG images (Figures 3b and 6) spread and merge into each other and thus produce the broad HG image. Near the edge of the HG (Figure 7) the image spread is compatible with that of the star image (Figure 2). The electron beam readout was nearly parallel (15°) to the line of HG (Figure 3b). This means that the lateral image spread of a small linear chain of beads was accentuated due to contributions of spread signals of adjacent sources.

It should be noted in passing that the HG light distribution as read out from the vidicon will not change radically as the HG intrinsic brightness decreases. To the first order, the vidicon signal is proportional to the total energy deposited on the photocathode rather than the level of luminous flux when the system is operated in the integration mode. Therefore, a given DN level requires the same number of scattering events in the HG source region but must accumulate them over a longer time.

If the S-6 HG were due to surface scattering by 50μ grains then the maximum intrinsic source luminance would have been L_o (line) $\simeq 12$ cd cm^{-2} which is five times less than L_o (line) $\simeq 65$ cd cm^{-2} for S-7 if the surface grains were scattering, and 200 times more than directly computed ($\simeq 0.26$ cd cm^{-2}).

The extra cloud heights required to interpret the late stage S-7 and S-6 HG's suggest that other charging mechanisms are operating which supplement the charging mechanism proposed by Criswell (1972) for early-stage levitation. Superthermal (>340 eV) solar wind electrons observed by Ogilvie *et al.* (1971) may accrete and enhance the surface fields. Scale lengths of the multipole electric fields greater than 10's of centimeters are required for the late stage HG. The >10 cm extensions of the HG also suggest the areal monopole fields may be important directly and also through a two-stage charging mechanism in levitating grains.

5. Surveyor Inter-Comparisons

Group III (Figure 6) compares the first frames of the HG as seen on missions S-7, 1, 5, 6 arranged along a different log-scale than Group II (Table I). The absence of corona in S-7 frame is probably due to both variations in coronal intensity as well as the greater luminance of the HG. The coronal temporal decay curve (Bohlin, 1971) parallels the S-7 curve somewhat (Figure 5) with the HG always much brighter than the corona because of the HG's proximity. Only after the S-7 HG fully decayed, was the corona visible on S-7 frames. As can be easily seen, S-5 has a horizontal extent which is clearly the result of HG. The bright yellow spot on S-1 is probably also HG.

Surveyor 5 apparently detected HG at a reasonably early stage, approximately 15 min after local sunset (Figure 5). However, reference to analog representation (Figure 8) reveals the same lack of details as in the S-6 case. R. Batson (personal communication, 1973) estimates the horizon distance as 2 km or slightly less. The

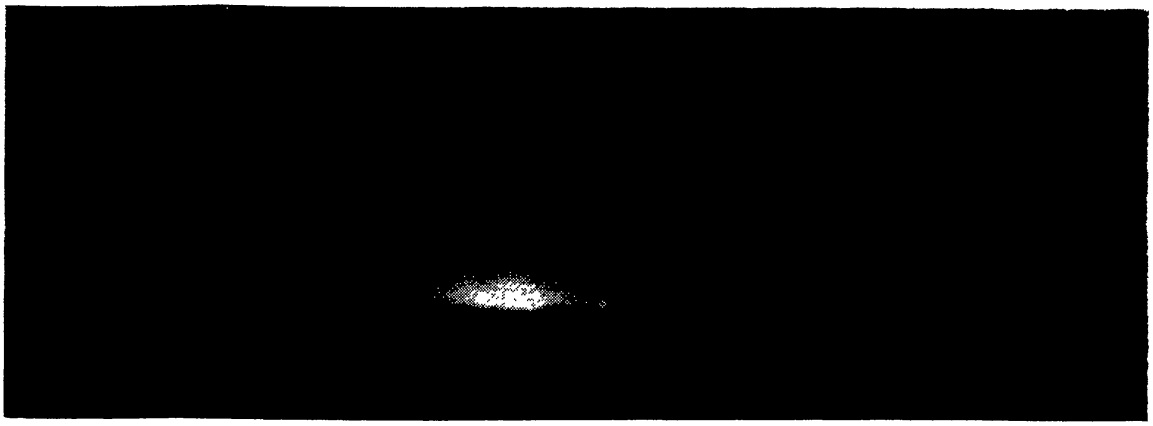

Fig. 8.

Fig. 9.

observed luminance at $11^h10^m55^s$ GMT on 24 September 1967 was $L_o \simeq 0.019$ cd cm^{-2}. Using the same geometric correction factors as for S-6, we have L_o (point) $\simeq 0.05$ cd cm^{-2} and L_o (line) $\simeq 0.1$ cd cm^{-2}. This is compatible with the early stage S-7 luminance ($L_o \simeq 0.26$ cd cm^{-2}).

There is some question as to whether or not S-1 detected HG. Norton *et al.* (1967) contended the solar corona was more extended along the horizon than one would expect. This can be seen in Figure 9 which was taken at 100 mm focal length. In addition, there is a bright spot which is clearly detected only on frame 165 day $15^h46^m11^s$ taken a few minutes after sunset. The observed luminance is 0.0393 cd cm^{-2}.

Some detail is observable in the horizon photography and a high resolution Orbiter photo of the S-1 spacecraft landing site does indicate slopes west of the spacecraft closer than 2 km (JPL Surveyor Project Final Report TR-32-1265, 1968). For a point source at 2 km and 10 cm high L_o(S-1) $\simeq 0.1$ cd cm^{-2}. This is compatible with early-stage S-7 luminance.

6. Conclusion

Electrostatic transport of lunar surface material was first suggested by Gold (1955). The suggested driving mechanism was transient charge separation due to photoelectron

ejection from the fully sunlit surface. Subsequent theoretical studies concluded that under daytime conditions the grains could at best rise only a few millimeters above the soil (Gold, 1962, 1966; Singer and Walker, 1962; Heffner, 1965). However, these studies did not anticipate the occurrence of dust churning in the terminator zone as observed by the Surveyor spacecraft. The key conceptual innovation suggested by Criswell (1972) was the retention of large differences of electrical surface charge across light/dark boundaries due to the highly resistive nature of the lunar surface. More recent work by Gold (1971) and Gold and Williams (1973) indicates the occurrence of a surface transport mechanism controlled by secondary electron emission and driven by low energy (500–1000 eV) electrons impacting the earthward lunar surface while the Moon is in the magnetotail. Secondary emission may be significant in the production of HG by creating very large and long lived electrical charge imbalances on individual grains, thus decreasing the intensity of the electric field required for grain levitation. However, the secondary emission mechanism cannot directly produce HG because the electric fields it creates are confined to the micron scale. Additionally, the Moon was probably not in the magnetotail during the Surveyor-7 observations of HG.

Observations of the lunar HG by the Surveyor spacecraft were completed before the first manned lunar landing. Unfortunately, no surface operations were conducted in the terminator zone and the small scale height of the glow ($\leqslant$20–30 cm) precluded its detection by orbiting instruments designed for other purposes. It is strange that no obvious patterns have been seen in the lunar soil which relate to the motion of surface dust required to produce HG. One would expect some patterns due to the symmetry imposed by shadow lines during sunset (Gold, private communication). Such patterns may exist but the areas where they would be obvious could have been missed during the Surveyor and Apollo missions. Active HG regions constitute only a small fraction of the surface and would tend to occur on slopes which were avoided by the astronauts. This must be considered an open question requiring more study.

Severny *et al.* (1973) have reported the detection of a lunar sky background at 5400 Å and 2700 Å during lunar day by a photometer on board Lunokhod-2. The 5400 Å background was also observed when the Sun was 1° below the local horizon and the horizon shadow was 700 m above Lunokhod-2. This means scattering grains were ejected by some means nearly 1 km above the terminator lunar surface. Severny *et al.* (1973) contend that a concentration of 10^{-8} particles cm^{-3} of 10–50 μ particles would be necessary to produce the sky brightness. However, assuming the particles are locally produced and vertically propelled in some manner to 1 km of altitude requires a surface ejection rate 10^4 times greater than the rate at which particles in this same size range are disturbed during regolith formation (Hartung *et al.*, 1972). Clearly, major mysteries still exist concerning material transport on the lunar surface and transport mechanisms other than those considered in this paper may be operative.

Electrostatic dust motion totally dominates (by 10^7) micrometeoritic churning in the source regions of horizon glow. The primary question to be considered next is the relative importance of the two mechanisms over regions of a square kilometer or more in controlling the distribution of lunar surface fines. The smoothing and layering

tendency of electrostatic transport opposes the tendency of micrometeorites to homogenize the surface. Two approaches must be employed. Theoretical modeling of electric field production will permit one to trace the evoked dust motions for specific geometries of the lunar surface about the Surveyor and manned landing sites. These models would provide a reasonable estimate of electrostatic layering about specific lunar samples and, in particular surface photographs. Finally, experiments should be formulated for deployment on both future Soviet surface vehicles and American orbital missions to determine the variation of mass transport rates or churning rates for specific locations on the Moon by direct detection of horizon-glow in both the visible near ultraviolet, and infrared.

Acknowledgment

The authors express sincere appreciation to Dr J. A. O'Keefe (Goddard Space Flight Center) and Prof. T. Gold (Cornell Univ.) for their long-standing encouragement and especially their challenging and constructive criticism during the course of this research.

References

Allen, C. W.: 1955, *Astrophysical Quantities*, University of London, The Athlone Press.
Allen, Harold L.: 1968, Surveyor Project Final Report – Part II: Science Results, JPL Tech. Report 32-1265, pp. 459–465.
Allen, L. H. and Salomon, P. M.: 1970, *J. Soc. Motion Picture Tel. Eng.* **79**, 615–620.
Bohlin, J. D.: 1971, *Solar Phys.* **18**, 450–457.
Braslau, D.: 1970, *J. Geophys. Res.* **75**, 3987–3999.
Criswell, D. R.: 1972, *Proc. Third Lunar Science Conf., Suppl. 3, Geochim. Cosmochim. Acta* **3**, 2671–2680.
Criswell, D. R.: 1973, 'Horizon Glow and the Motion of Lunar Dust', in R. Grard (ed.), *Photon and Particle Interactions with Surfaces in Space*, D. Reidel Publ. Comp., Dordrecht, Holland, pp. 545–556.
Dohnanyi, J. S.: 1971, *Science* **173**, 558.
Gault, D. E., Adams, J. B., Collins, R. K., Kuiper, G. P., O'Keefe, J. A., Phinney, R. A., and Shoemaker, E. M.: 1968 'Post-Sunset Horizon Glow', Surveyor Project Final Report – Part II: Science Results.
Gault, D. E., Adams, J. B., Collins, R. K., Kuiper, G. P., Masursky, H., O'Keefe, J. A., Phinney, R. A., and Shoemaker, E. M.: 1970, *Icarus* **12**, 230–232.
Gold, T.: 1955, *Monthly Notices Roy. Astron. Soc.* **115**, 585–604.
Gold, T.: 1962, 'Processes on the Lunar Surface', in Z. Kopal and Z. Michailov (eds.), *Proc. IAU Pulkovo Meeting*.
Gold, T.: 1966, 'The Moon's Surface', in W. H. Hess, D. H. Menzel, and J. A. O'Keefe (eds.), *The Nature of the Lunar Surface*, John Hopkins Press, pp. 107–121.
Gold, T.: 1971, *Proc. Second Lunar Science Conf., Geochim. Cosmochim. Acta, Suppl. 2*, **3**, 2675–2680.
Gold, T.: 1973, 'Particle Interactions with Celestial Objects: Concluding Remarks', in R. Grard (ed.), *Photon and Particle Interactions with Surfaces in Space*, D. Reidel Publ. Co., Dordrecht, Holland, pp 571–576.
Gold, T. and Williams, G. J.: 1973, 'Electrostatic Transportation of Dust on the Moon', in R. Grard (ed.), *Photon and Particle Interactions with Surfaces in Space*, D. Reidel Publ. Co., Dordrecht, Holland, pp. 557–560.
Hartung, J. G., Hörz, F., and Gault, D. E.: 1972, *Proc. Third Lunar Science Conf., Suppl. 3, Geochim. Cosmochim. Acta.* **3**, 2735–2753.
Heffner, H.: 1962, Minn. Univ. Report of August 1962 TYCHO meeting (N66-16171).

Johnson, F. S., Carroll, J. M., and Evans, D. E.: 1972, *Proc. Third Lunar Science Conf., Suppl. 3, Geochim. Cosmochim. Acta.* **3**, 2735–2753.
Norton, R. H., Guinn, J. E., Livingston, W. C., Newkirk, G. A., and Zirin, H.: 1967, *J. Geophys. Res.* **72**, 815–817.
Ogilvie, K. M., Scudder, J. D., and Sugiura, M.: 1971, *J. Geophys. Res.* **76**, 8165–8173.
O'Keefe, J. A., Adams, J. B., Gault, D. E., Green, J., Kuiper, G. P., Masursky, H., Phinney, R. A., and Shoemaker, E. M.: 1968, Surveyor VI Mission Report – Part II: Science Results, JPL Tech. Rept. 32-1262, pp. 171–176.
Olhoeft, G. R., Frisillo, A. L., and Strangway, D. W.: 1972, in J. W. Chamberlain and C. Watkins (ed.), *The Apollo 15 Lunar Samples*, Lunar Science Inst., Houston, Tex., p. 575.
Rennilson, J. J.: 1968, Surveyor Project Final Report – Part II: Science Results, JPL Tech. Report 32-1265, pp. 119–121.
Rennilson, J. J.: 1969, JPL Tech. Report 32-1443, pp. 165–175.
Rosenburg, G. V.: 1970, *Soviet Astron. AJ.* **14**, 361–363.
Severny, A. B., Terez, E. I., and Avereva, A. M.: 1973, *COSPAR Report i. 17, #25*, Konstanz, Germany.
Singer, S. F. and Walker, E. H.: 1962, *Icarus* **1**, 112–120.
Thorpe, T. E.: 1973, *Appl. Opt.* **12**, 359–363.
Van de Hulst, H. C.: 1957, *Light Scattering by Small Particles*, John Wiley and Sons.